Available online at www.sciencedirect.com

SciVerse ScienceDirect

journal homepage: www.elsevier.com/locate/he

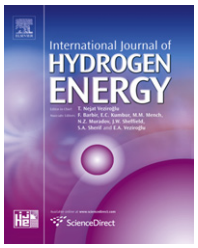

Pt_3Y electrocatalyst for oxygen reduction reaction in proton exchange membrane fuel cells

Sung Jong Yoo [a], Kug-Seung Lee [a], Seung Jun Hwang [a], Yong-Hun Cho [b], Soo-Kil Kim [c], Jeong Woo Yun [d], Yung-Eun Sung [e], Tae-Hoon Lim [a,*]

[a] Fuel Cell Research Center, Korea Institute of Science and Technology, 39-1 Hawolgok-dong, Seoul 136-791, Republic of Korea
[b] School of Advanced Materials Engineering, Kookmin University, 861-1 Jeongneung-dong, Seoul 136-702, Republic of Korea
[c] Department of Integrative Engineering, Chung-Ang University, 221, Heukseok-Dong, Dongjak-Gu, Seoul 156-756, Republic of Korea
[d] School of Applied Chemical Engineering, 300 Yongbong-dong, Buk-gu, Gwangju, Republic of Korea
[e] World Class University Program of Chemical Convergence for Energy & Environment, School of Chemical and Biological Engineering, Seoul National University, Shinlimdong 56-1, Seoul 151-742, Republic of Korea

ARTICLE INFO

Article history:
Received 12 December 2011
Received in revised form
16 February 2012
Accepted 17 March 2012
Available online 14 April 2012

Keywords:
PtY alloy
Sputtering technique
Proton exchange membrane fuel cells
Utilization of catalysts
Multilayer MEA

ABSTRACT

We report here that significant electrocatalysis occurs during oxygen reduction reaction (ORR) at the Pt_3Y alloy thin film electrodes. In addition, we synthesized Pt_3Y alloy nanocatalysts for use in proton exchange membrane fuel cells, fabricated by using a high pressure sputtering technique in a gaseous mixture of Ar and He. Rather than the dense film deposited by conventional sputtering techniques, the resulting structure was comprised of a Pt_3Y alloy nanocatalyst layer with an average particle size of 10–12 nm. The Pt_3Y alloy nanocatalysts were characterized by scanning electron microscopy, transmission electron microscopy, high-resolution X-ray photoelectron spectroscopy, and X-ray absorption near edge spectroscopy. The cell performance of the membrane electrode assembly with multiple layers of sputter-deposited Pt_3Y alloy nanoparticles and spray-deposited Nafion–carbon-ink improved dramatically compared to that obtained with the Pt only nanoparticles. The high performance of Pt_3Y alloy nanocatalysts fabricated at a sputtering pressure of 200 mTorr (Ar/He = 1) was due to miniaturization of the Pt_3Y alloy particles, formation of the porous catalyst layer, and enhancement of the kinetic activity for ORR.

1. Introduction

Proton exchange membrane fuel cells (PEMFCs) are promising and worthy candidates for high efficiency and low emission energy conversion devices in mobile, stationary and portable application sectors [1–3]; however, many problems still need to be solved, the major one being the reduction of the significant overpotential for the oxygen reduction reaction (ORR) in the PEMFCs. The strategies to improve ORR kinetics are diverse, ranging from the bi-metallically alloying with transition metals [1,4–9]. Recently, studies on Pt-based bi-metallic alloys have been conducted on the correlation between the modified surface electronic structure of Pt affected by the second transition metal and catalytic activity for the ORR [10–13]. Another tremendous challenge is to reduce the amount of electrocatalyst required without sacrificing

* *Corresponding author*. Tel.: +82 2 958 5201; fax: +82 2 958 5119.
E-mail addresses: thlim@kist.re.kr, kistfc@gmail.com (T.-H. Lim).
0360-3199/$ – see front matter Copyright © 2012, Hydrogen Energy Publications, LLC. Published by Elsevier Ltd. All rights reserved.
doi:10.1016/j.ijhydene.2012.03.089

performance. One important approach is to form catalyst layers by using direct sputter deposition. Hirano et al. deposited a Pt layer (0.1 mg/cm^2), as a cathode electrode, using a sputter technique on an uncatalyzed gas diffusion layer (GDL). This modification resulted in enhanced cell performance [14]. O'Hayre et al. deposited a Pt layer on the Nafion 117 using a sputtering technique. In this system, cell performance at a loading of 0.04 mg/cm^2 (Pt) was compared to a commercial membrane electrode assembly (MEA) with a platinum loading of 0.4 mg/cm^2 (Pt) [15]. However, conventional sputtered Pt catalyst layers suffered from the deposition of Pt as a conformal film on the substrate [16]. Due to this compact and dense structure, the Pt catalyst layer was not porous, and displayed a small electrochemical active surface (EAS) area. In the previous work, we have reported that a high pressure (200 mTorr) sputtering technique could produce nanoscale Pt particles, which form in the vapor as a result of the high pressure [17]. This resulted from the subsequently collisions, nucleation, and growth of the sputtered atoms in the vapor at these high pressures. This high-pressure sputtering technique leaded to an improvement in the Pt microstructure, such that the Pt catalysts layer was more porous, allowing enhancedPt utilization.

In this paper, we report a more active electrocatalytic cathode material comprising Pt-based alloys made of Y. In particular, we synthesized Pt_3Y alloy nanocatalysts deposited using a high-pressure radio frequency (RF) magnetron co-sputtering technique with a mixture of gaseous Ar and He for use in PEMFCs. Nanoscale Pt_3Y alloy particles were achieved using a sputtering pressure (200 mTorr) and were characterized by scanning electron microscopy (SEM), transmission electron microscopy (TEM), X-ray diffraction (XRD), high-resolution X-ray photoelectron spectroscopy (HR-XPS), and X-ray absorption near edge spectroscopy (XANES). Single cell performance of MEA utilizing the synthesized Pt_3Y alloy nanoparticles was analyzed.

2. Experimental

2.1. *Electrochemical characterization using a rotating disk electrode*

Pt_3Y alloy thin film electrodes were grown using an RF magnetron co-sputtering system comprising a dual sputtering gun. Si (100) and glassy carbon were used as substrates to characterize the structural and electrochemical properties, respectively. Co-sputtering was performed under inert Ar gas at a flow rate of 26 sccm at room temperature for 10 min, and this produced films with a thickness of approximately 100 nm. Before examining the catalytic activity and stability, the electrodes were characterized by Auger electron spectroscopy (AES) in a scanning Auger nanoprobe (ULVAC PHI-700). The sample surface was sputtered for 5 s before AES measurements. The AES spectra were recorded using a 3 keV accelerating voltage with a spot size of 150 μm, recorded over the range 20–2420 eV. The chamber was held at a base pressure below 5×10^{-10} Torr. Fig. 1 shows the Auger spectra for the Pt–Y electrodes, respectively. Evidently all the peaks correspond to those characteristic of Pt and Y. According to these

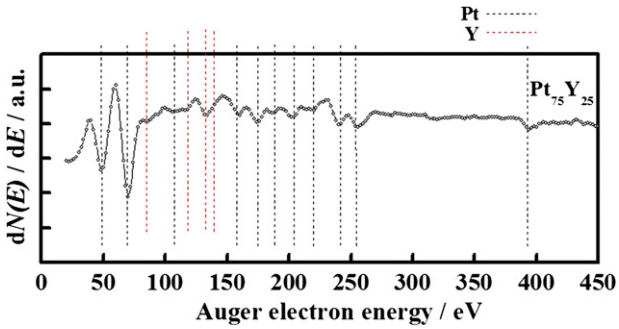

Fig. 1 – AES spectrum of a Pt_3Y electrode.

spectra, in the near surface region the compositions of the Pt-Y electrodes were ~75% Pt and ~25% Y.

An AutoLab PGSTAT20 potentiostat and a rotating disk electrode (RDE) system (Ecochemie) with a conventional three-electrode configuration were used for all the electrochemical measurements. All the electrochemical measurements, except for the ORR with the RDE configuration, were performed in an Ar-purged 0.1 M $HClO_4$ solution. For the ORR experiment, 99.99% oxygen gas was bubbled into the electrolyte for 60 min before each measurement. A catalyst-coated glassy carbon electrode with a diameter of 5 mm was used as the working electrode. Before each measurement, the glassy carbon electrode was polished with a 0.05-μm alumina paste followed by washing with distilled water in an ultrasonic bath. A saturated calomel electrode (SCE) with 3 M KCl (Gamry) and a glassy carbon rod were used as the reference and counter electrodes, respectively.

The ORR measurements were performed in 0.1 M $HClO_4$ solutions under flow of O_2 (research grade) using the glassy carbon RDE at a rotation rate of 1600 rpm and a sweep rate of 10 mV s^{-1}. In order to produce a clean electrode surface, several potential sweeps between 0.05and 1.1 V vs. RHE were applied to the electrode prior to the ORR measurement. In the ORR polarization curve, current densities were normalized in reference to the geometric area of the glassy carbon RDE (0.196 cm^2).

For the ORR at an RDE, the Koutecky–Levich equation can be described as follows:

$$1/i = 1/i_k + 1/i_{l,c} = 1/i_k + 1/\left(0.62nFAD_0^{1/2}\omega^{1/2}\nu^{-1/6}C_0^*\right) \quad (1)$$

where i is the experimentally measured current, $i_{l,c}$ is the diffusion-limiting current, and i_k is the kinetic current; where D_0 is the diffusivity of oxygen in 0.1 M $HClO_4$ (estimated from the product of O_2 diffusivity at infinite dilution and the ratio of the dynamic viscosities of the electrolyte and pure water), n is the number of electrons in the O_2reduction reaction (*i.e.*, $n = 4$), ν is the kinematic viscosity of the electrolyte, c_0 is the solubility of O_2 in 0. 1 M $HClO_4$, and ω is the rotation rate. Then, the kinetic current was calculated based on the following equation:

$$i_k = (i \times i_{l,c})/(i_{l,c} - i) \quad (2)$$

For each catalyst, the kinetic current was normalized to the real surface area (0.202 cm^2; see Fig. 3).

2.2. Fabrication of Pt_3Y alloy nanoparticles using the sputter technique

The Pt_3Y alloy nanoparticles deposited on a GDL were fabricated using an RF magnetron sputter technique at high pressure. Pt (Pt 99.99%, United Vacuum & Materials) and Y (Y 99.99%, United Vacuum & Materials) were used as the target materials. The base pressure was less than 1×10^{-6} Torr and the working pressure was 200 mTorr. The working distance between the sputter target and substrate was 26 cm. Sputtering was carried out under an atmosphere of Ar and He (volume ratio of 1:1) at room temperature. The amount of sputtered Pt_3Y alloy nanoparticles produced was calculated from the weight change in the amount of loaded Pt; the amount of Pt nanocatalyst could be controlled by sputtering working pressure, time, and RF power.

2.3. Structure characterizations

Structural analyses were carried out using TEM, XANES, HR-XPS, XRD, and SEM. TEM images were obtained using a JEOL EM-2000 EX II microscope at an accelerating voltage of 200 kV. Cu grids were used as the substrate and for TEM analysis. The morphology of all samples was carefully measured by planar-sectional SEM (JEOL 6330F). $Pt L_{III}$ edge XANES were recorded using the 3C1 beam line at the Pohang Light Source (PLS) with a ring current of 120–170 mA at 2.5 GeV. A Si(111) monochromator crystal was used after detuning the intensity to 85% to eliminate high-order harmonics. The data were collected in fluorescence and transmission modes. Energy calibrations were carried out for all measurements by placing Pt foil in front of the third ion chamber and assigning the first inflection point to 11,564 eV. HR-XPS measurements were performed on the soft X-ray beam line (8A1) connected to an undulator (U7) at the PLS. The end station was composed of a high performance electron analyzer (SCIENTA-200) with energy and angular resolution of 5 meV and 0.5°, respectively. The experiment was carried out in an ultrahigh vacuum chamber with a base pressure $\leq 5 \times 10^{-10}$ Torr. All spectra were measured using 630 eV of incident photon energy. XRD (MAC Science M18XHF-SRA equipped with a Cu Kα source at 30 kV–30 mA) analysis of Pt_3Y electrode was used to determine the degree of crystallinity.

2.4. Preparation of catalyst layer with multi Pt_3Y alloy layers

Nafion–carbon-ink is prepared by first mixing an appropriate amount of isopropanol and carbon in the 50 ml reactor for 15 min. The required amount of Nafion–carbon solution is then added and mixed until the homogenous mixture is obtained. An appropriate amount of solvent is removed to obtain the Nafion–carbon-ink. Both sides of the carbon cloth are printed the Nafion–carbon-ink using the spray method and dried in the oven at 160 °C for 2 h. The carbon cloth with Nafion–carbon-ink layer is placed on the holder designed by the author in the sputtering chamber and the chamber pressure is pumped to reach 1×10^{-6} Torr. The Pt and Y plasmas are deposited on the Nafion–carbon-ink layer to form an active Pt_3Y alloy nanocatalyst thin layer.

2.5. Electrochemical and fuel cell testing

Performance of PEMFCs that used the sputtered Pt and Pt_3Y alloy nanocatalysts was evaluated by measuring cell voltage of a 1-cm^2 cross-section of the catalyst zone under constant current conditions with a potentiometer. The single cell consisted of two graphite plates with serpentine flow-fields and two metal end-plates adjacent to the graphite plates. The MEA fabricated in this study was formed using Nafion 112 as the polymer electrolyte membrane. Before use, Nafion 112 was pretreated in a hydrogen peroxide solution (3 wt.%) for about 1 h at 100 °C followed by washing in deionized water for 1 h. The procedure described above was repeated, and the membrane then was boiled in a sulfuric acid solution (0.5 M) for 1 h and washed in boiling deionized water for 1 h. The prepared GDL and MEA were placed between two graphite plates, which then were assembled using the appropriate pressure. For the performance measurements, a humidified hydrogen and oxygen, at stoichiometric ratio of 1.5:2, was fed to the anode and cathode side of the single cell at a temperature of 75/70 °C. During the measurement, the temperature was maintained at 70 °C and the pressure was held constant at atmospheric pressure. The cell voltage of each sample was obtained with increasing current density using a fuel cell test station (FCTS, Won-a tech) to measure the current–voltage curves.

Based this sputtering new technique, we carried out the electrochemical performances of PEMFCs single cells of Pt_3Y and pure Pt electrocatalyst. In all cases, the amounts of Pt nanocatalysts deposited by using sputtering technique (0.1 mg/cm^2) were added to the anode and the amounts of Pt_3Y (0.03, 0.06, and 0.12 mg/cm^2) were added to the cathode. Fuel cell performance curves were measured after allowing for a steady reading at each point during the current scan, as controlled by the fuel cell test station. The open circuit voltage of all samples sputtered showed an open circuit voltage of 1.0–0.9 V, which is close to that of commercial Pt catalysts.

3. Results and discussion

3.1. Electrochemical and structure characterization of the Pt_3Y alloy thin film

The bulk composition of Pt_3Y electrode was verified using X-ray diffraction. The results of these measurements are shown Fig. 2, along with the reference pattern for Pt_3Y. The patterns for Pt_3Y corresponded to the respective reference traces for this compound, from the powder diffraction file database. According to these data, the majority of the electrode was compromised of a single intermetallic phase, with no significant secondary phase present. Before the ORR was evaluated on the Pt_3Y alloy thin film electrodes, we have estimated the real surface area of sputter-deposited Pt_3Y alloy thin film electrodes on glass carbon by using CO-stripping measurement as following the procedures. The 0.1 M $HClO_4$ solution was purged with Ar gas for 30 min prior to electrochemical measurements. For CO-stripping measurements, pure CO was bubbled into the electrolyte under potential control at 0.1 V vs. NHE for 30 min. Then, the electrolyte was

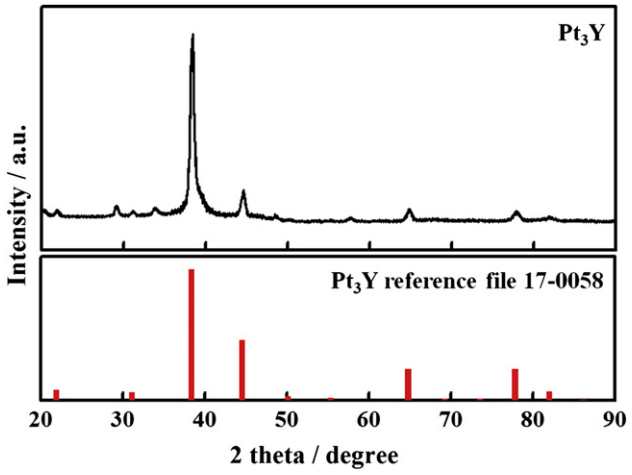

Fig. 2 – X-ray diffraction traces of Pt_3Y.

purged for 30 min with Ar gas, while keeping the electrode potential at 0.1 V vs. NHE to eliminate the dissolved CO in the electrolyte. The first anodic scan (scan speed: 10 mV/s) was performed to electro-oxidize the adsorbed CO and the subsequent voltammetries in order to verify the completeness of the CO oxidation. Assuming that each Pt surface atom is covered by a single adsorbed CO molecule, the charge for electro-desorption of CO should be 420 μC/cm. Fig. 3 shows the voltammograms of Pt_3Y in the presence and the absence of CO. The integrated CO stripping charge for all voltammograms came to 85 ± 5 μC, irrespective of the electrode composition. This suggests that the geometric (0.196 cm^2) and real surface areas are almost equal (about 0.202 ± 0.01 cm^2).

We now report the electrochemical characterization and enhanced ORR activity of Pt_3Y alloy and Pt thin film electrodes. The electrocatalytic properties of the Pt_3Y alloy thin film electrode were benchmarked toward the ORR against a pure Pt thin film electrode. Fig. 4 displays polarization curves of the

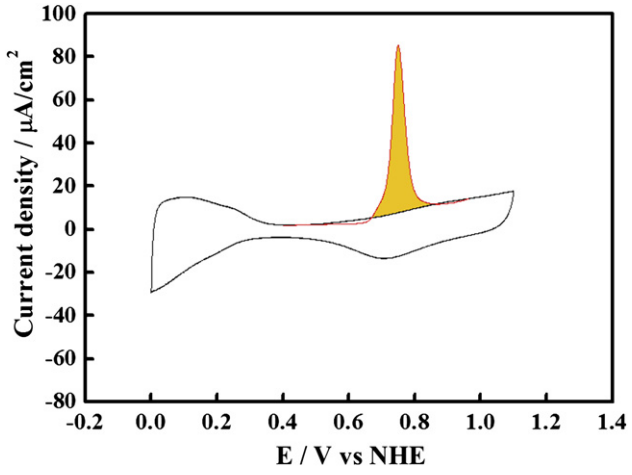

Fig. 3 – CO stripping voltammetry of Pt_3Y after CO adsorption at 0 V vs. NHE for different adsorption times. During CO stripping Ar in working electrode compartment (flow rate 120 ml min^{-1}). Sweep rate 10 mV/s. Room temperature.

ORR on Pt_3Y alloy (red) and Pt thin film (black) electrodes in 0.1 M $HClO_4$ at 293 K Pt_3Y alloy electrode exhibited dramatically increased half-wave potentials relative to the corresponding pure Pt electrode; in other words, the half-wave potentials of Pt and Pt_3Y alloy thin film electrodes were 843 and 941 mV (vs. RHE), respectively (Fig. 4). The kinetic current (j_k) (see Experimental section) was calculated by the Koutecky–Levich equation and normalized in reference to the real surface area (Fig. 3). At 0.9 V, the ORR activity of Pt_3Y alloy was enhanced by factors of 16 times relative to pure Pt (see Fig. 5).

In order to reveal the nature of the stability of Pt_3Y alloy catalyst used in electrocatalytic oxygen reduction, we conducted the comparison of the first steady cycle (black line) and after 3000 cycles (red line), for Pt_3Y alloy electrode in an electrochemical environment. The stability effect for Pt_3Y was determined with an accelerated stability test by continuously applying linear potential sweeps from 0.6 to 1.1 V, which caused surface oxidation/reduction cycles of Pt. This potential region generally occurred during the metal dissolution and surface oxide formation. As shown in the Fig. 6 and Fig. 7, Pt_3Y alloy catalysts showed little change in activity and in composition after 3000 cycles. This indicates that the Pt_3Y alloy catalyst has been designed for ORR with high activity and long-term stability.

To determine the competing influences in this result, it is necessary to understand the ORR mechanism. The ORR mechanisms are associated with a reaction wherein oxygen adsorbed on the catalyst binds with an electron and a proton; further, several intermediates (O, OH, OOH) are involved in the ORR along with the reactant, oxygen, and the final product, water. The ORR involves both the breaking of the O–O bond and the formation of an OH bond, which is a well-known ORR inhibitor. In brief, the changes in the electronic structure of Pt

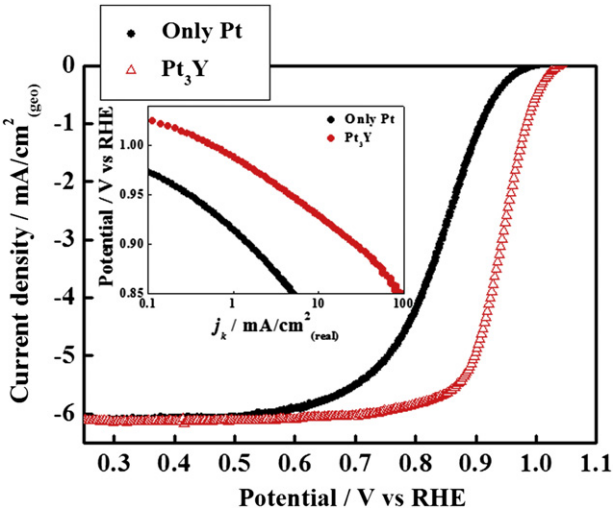

Fig. 4 – Oxygen reduction reaction (ORR) polarization curves using Pt_3Y alloy (red) and pure Pt (black) thin film electrodes in 0.1 M $HClO_4$ solution; the sweep rate was 10 mV/s and the rotation rate was 1600 rpm. The inlet shows the Tafel plots of Pt_3Y alloy (red) and pure Pt (black) thin film electrodes. (For interpretation of the references to colour in this figure legend, the reader is referred to the web version of this article.)

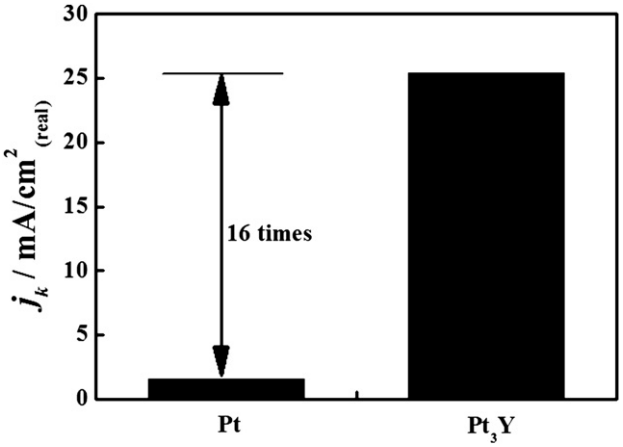

Fig. 5 – The specific activity of Pt_3Y alloy and pure Pt thin film electrodes expressed as a kinetic current density (j_k) for the ORR at 0.9 V.

during the alloying with Y facilitate the transition of the adsorbed OH to water by the modification of the binding energy of the oxygen-containing species (OCS). Further, an appropriate parameter such as the binding energy of Pt 4f can be helpful in discussing the electronic structure of Pt. We measured the binding energy of Pt 4f for all the alloys by using synchrotron-based HR-XPS.

The reactivity of any given metal (Pt) can be changed substantially by alloying. For Pt-based alloy catalysts used for the ORR, Pt is usually alloyed with 3d transition metals so as to downshift the d-band center of surface Pt atoms [18]. The position of the d-band center relative to the Fermi energy can be directly related to the binding energies of oxygen and its reaction intermediates. Shifting the d-band center for surface Pt, whose d-band is more than half-full, is well-known to be accompanied by a change in the surface core level shift (SCLS) in the same direction [19,20].

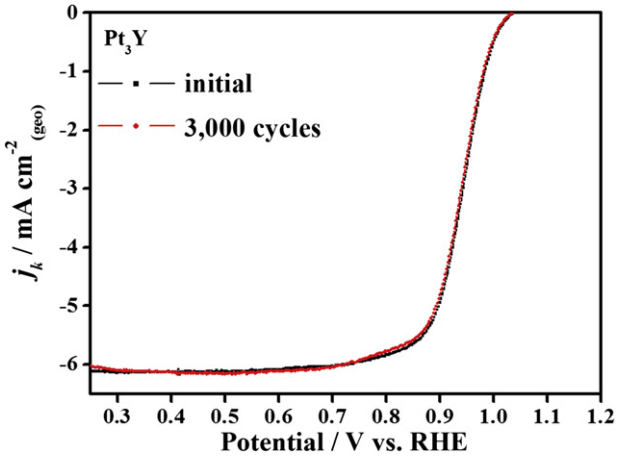

Fig. 6 – A comparison of the first steady cycle (black line) and after 3000 cycles (red line), for Pt_3Y alloy electrode. (For interpretation of the references to colour in this figure legend, the reader is referred to the web version of this article.)

HR-XPS was performed with Pt_3Y alloy and pure Pt samples. Fig. 8 compared the Pt 4f core level peaks of the Pt_3Y alloy and pure Pt samples. The core level peak of the Pt_3Y sample was shifted to a lower binding energy more so than the pure Pt samples. Since the XPS technique is not surface-sensitive at the monolayer level, this large shift (0.3 eV in binding energy) must be attributed to changes in the nearest neighbors surrounding the Pt atom. Moreover, the references 20 and 21 suggest that variation in the d-band center for metal overlayers is accompanied by a similar variation in the SCLS.

The low binding energy shift of the Pt_3Y alloy sample was further verified by XANES analysis in order to remove ambiguities in the HR-XPS analysis. Fig. 9 represents the Pt L_{III} edge of the Pt_3Y alloy sample. The XANES region of Pt L_{III} can be used for assessing qualitative changes in the fractional d-band occupancies of Pt, since the XANES region of the XAS spectrum is dependent mainly on multiple scattering and multi-photon absorptions [21]. As shown in Fig. 9, the number of Pt 5d holes in the case of Pt_3Y alloy is smaller than that in the case of pure Pt; in particular, the Pt 5d states in the Pt_3Y alloy hardly showed any variations. The small vacancy of the Pt

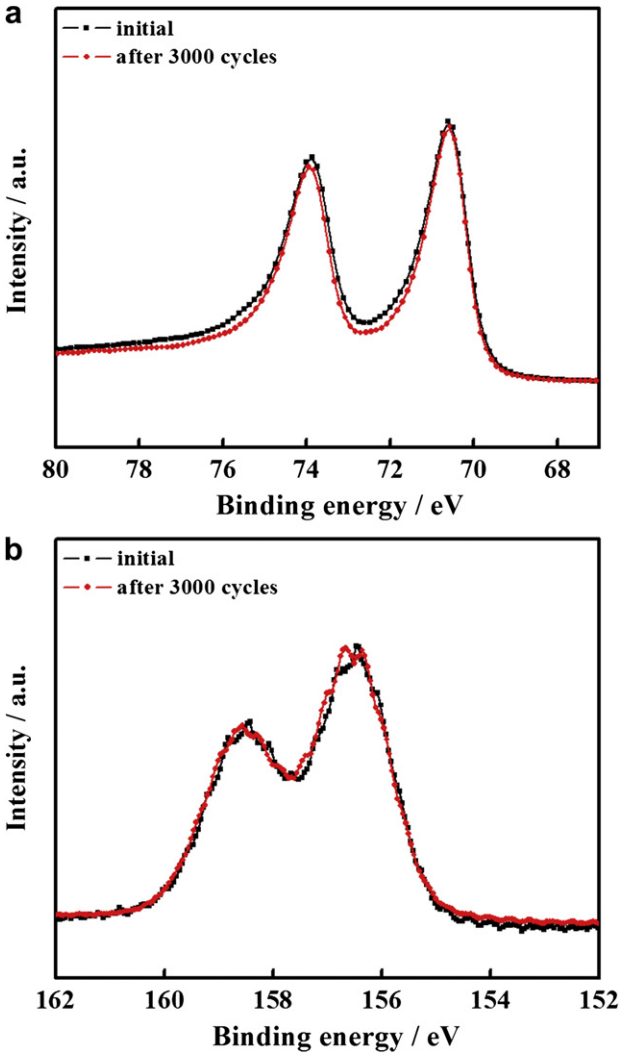

Fig. 7 – XPS spectra of Pt_3Y alloy catalysts before and after potential cycles. (a) Pt 4f peaks and (b) Y 3d peaks.

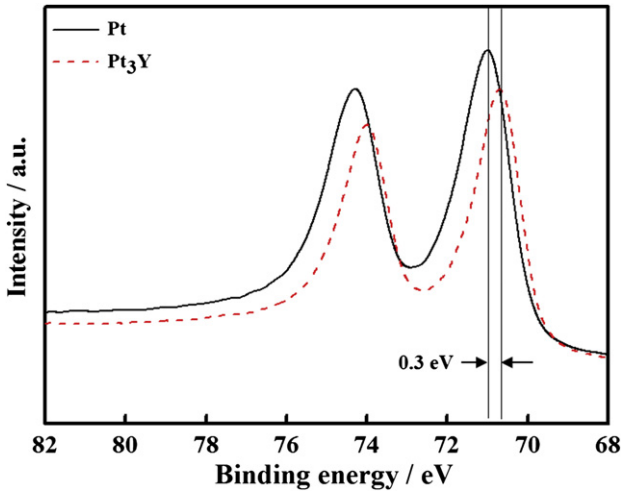

Fig. 8 – Pt 4f peaks of Pt_3Y alloy and pure Pt thin film electrodes.

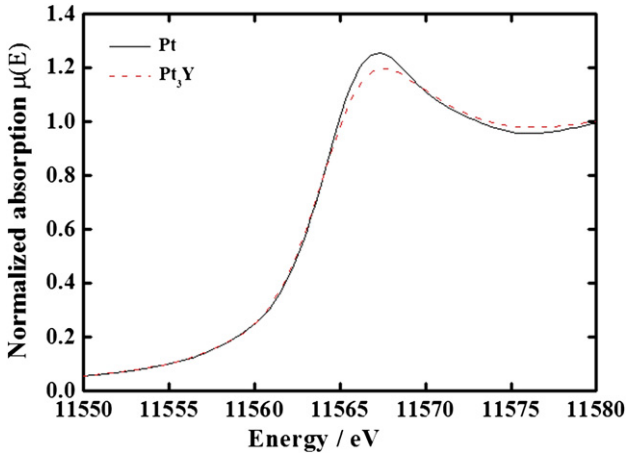

Fig. 9 – Normalized Pt L_{III} edge XANES spectra of Pt_3Y alloy and pure Pt thin film electrodes.

d-band means that the density of state of Pt is pulled from below the Fermi level to just above the metal Pt valence band, which widens the d-bandwidth and shifts the d-band center downwards in energy toward the Fermi level. In other words, Pt_3Y alloy electrodes grab O, OH and OOHslightly, speeding the desired oxygen-splitting reaction.

3.2. *Performance characterization of MEA with Pt_3Y nanoparticles as cathode catalysts*

In generally, the Pt-based alloy (PtNi, PtCo, PtFe, PtPd, etc.) nanocatalysts may be prepared into nanoparticles through colloidal alloying or impregnation alloying. Considering the high reduction potential ($Y^{3+} + 3e^- \rightarrow Y$; $E^0 = -2.23$ V) of Y,

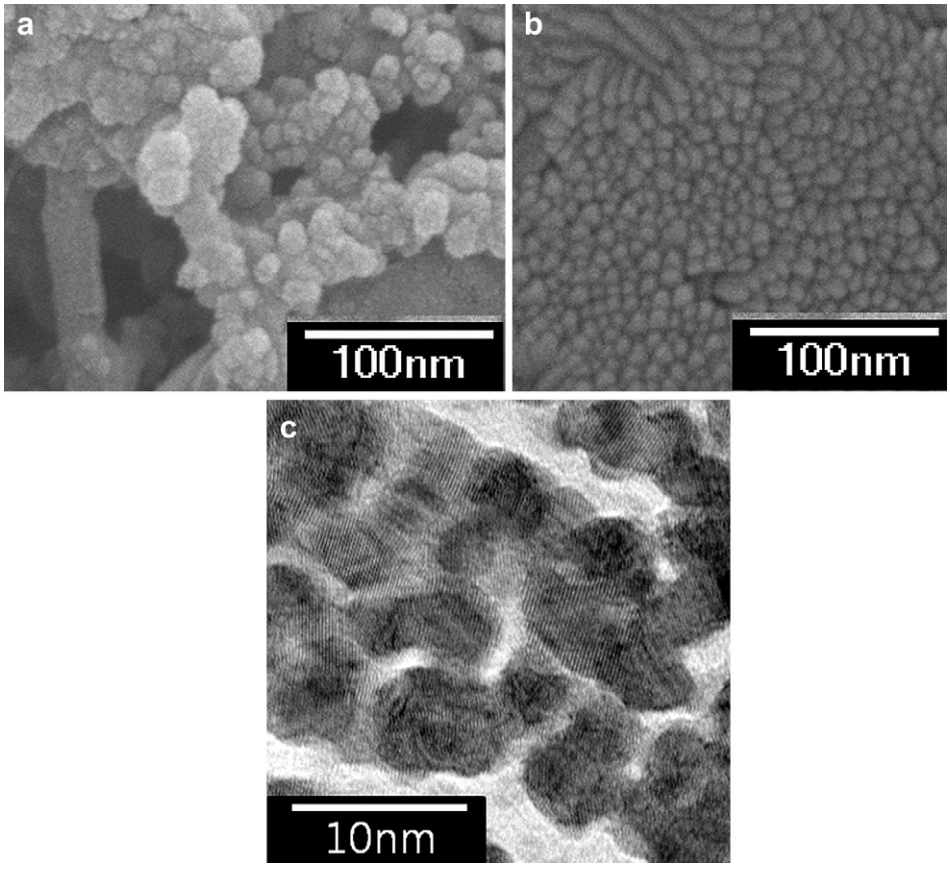

Fig. 10 – SEM images of Pt_3Y nanocatalyst layers deposited on the (a) GDL substrate and (b) Si (100) substrate, and (c) High-resolution TEM image of Pt_3Y nanocatalyst.

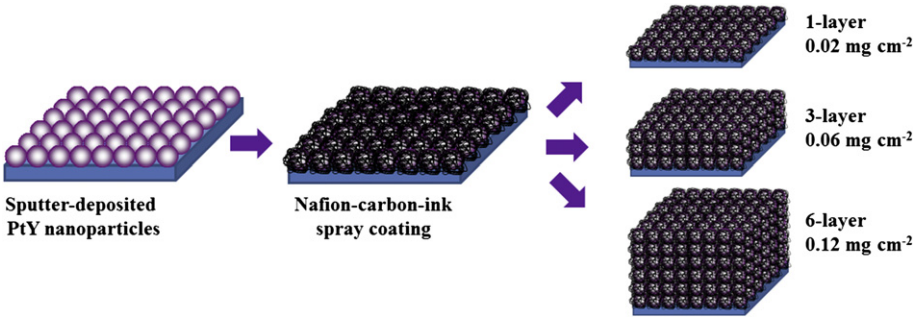

Fig. 11 – Schematic diagrams for the proposed catalyst multi-layers structure.

however, the Pt_3Y alloy nanocatalysts have been not synthesized by conversion chemical reduction methods. Herein, we suggest the new synthesis technique, that is, high-pressure co-sputter alloying technique. This co-sputter alloying technique allows the control of the size range and the composition of the Pt_3Y alloy nanoparticles through power control of two sputter guns and working pressure control.

To date, conventional sputtered Pt catalyst layers have suffered from the deposition of Pt as a conformal film on the substrate [16]. Due to this compact and dense structure, the Pt catalyst layer was not porous, and displayed a small electrochemical active surface (EAS) area. In the previous works, we have investigated Pt nanocatalysts deposited using a high pressure (200 mTorr) RF magnetron sputtering technique with a mixture of gaseous Ar and He for use in PEMFCs, which resulted in achieving the nanoscale Pt particles of 8 ± 2 nm. The size of Pt_3Y alloy particles prepared by the above method was confirmed by taking the HR-TEM images (Fig. 10(c)). The size of Pt_3Y alloy particles sputtered at 200 mTorr pressure with a mixture of gaseous Ar and He mixture gas was in the range of 10–12 nm, as shown in Fig. 10.

In addition, the processes should satisfy the following conditions; the access condition of triple phase boundary (TPB), where the electrolyte, gas, and electrically connected catalyst particles contact, and the water management at the cathode. In order to form an effective surface for the electrochemical reactions, the sputtered Pt_3Y alloy nanoparticles should be electrolytically connected with the Nafion membrane or Nafion inomer and electrically bound to each other. To increase the electrical conductivity, we added carbon powder to the Nafion solution. Therefore, our strategy for preparing the electrode was to apply Nafion–carbon-ink between the sputterings. Following this strategy, we prepared PEMFC electrodes and studiedthe electrochemical performance of PEMFC incorporating these electrodes. As shown Fig. 11, Nafion–carbon-inkwas simply sprayed on the Pt_3Y alloy surface deposited by using sputtering technique. The Nafion–carbon-ink/catalyst assembly was dried for 60 min in the vacuum sputter chamber to remove any residential solvent such as isopropyl alcohol and water. This procedure was repeated to finalize the formation of the Nafion–carbon-ink/catalyst layers. The multilayer electrodes of Nafion–carbon-ink/catalyst were used to determine the best utilization of the Pt_3Y alloy catalysts.

MEAs were prepared with multiple layers of sputter-deposited Pt_3Y alloy nanoparticles and spray-deposited Nafion–carbon-ink as shown in Fig. 11.The anode and cathode were built in an identical manner. Fig. 12 compares the performance of cells for which the anode and cathode is composed of one, three, and six sputter-deposited Pt_3Y layers

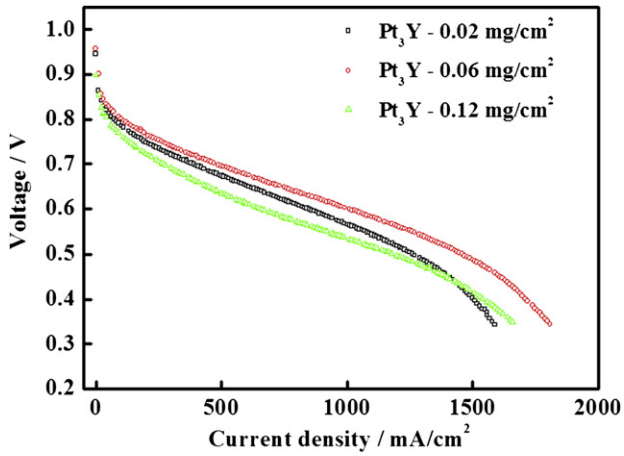

Fig. 12 – Polarization curves of MEAs with different Pt_3Y nanocatalyst loadings (0.02 mg/cm^2 (□), 0.06 mg/cm^2 (○), and 0.12 mg/cm^2 (Δ)).

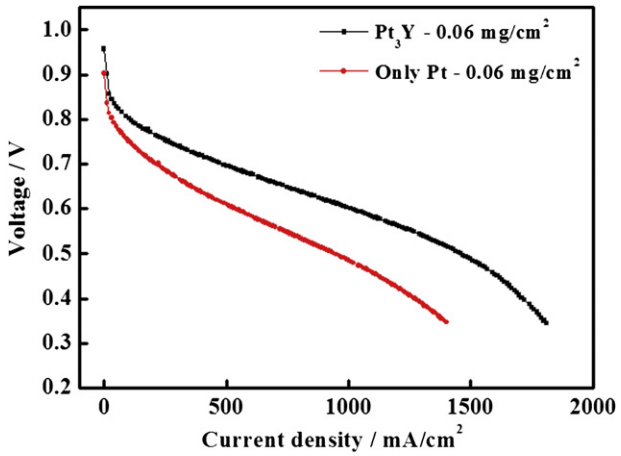

Fig. 13 – Polarization curves of MEAs with pure Pt nanocatalyst layers (-■-) and Pt_3Y nanocatalyst layers (-●-).

dispersed between Nafion–carbon-ink. Individual Pt_3Y alloy layers weight of one, three, and six resulted in electrode loadings of 0.02, 0.06, and 0.12 mg/cm^2, respectively. Fig. 12 shows that the performance of the electrodes improves with an increase in the number of sputterings, but this effect decreases quickly as the number increases further. Repeating the sputtering over six times did not bring any significant improvements but decrease the performance of the electrodes. In other word, the increase of Nafion–carbon-ink/catalyst layers no longer contributes to increasing the effective surface area. Fig. 13 demonstrates well the kinetic effect of the Pt_3Y alloy nanoparticles (104 mA/cm^2 at 0.8 V) on electrode performance, which improved dramatically compared to that obtained with the Pt only nanoparticles (27 mA/cm at 0.8 V). This result is in agreement with the result of half-cell test for ORR, as shown in previous Section 3.1. This indicates that significant electrocatalysis occurs during the ORR at the Pt_3Y alloy electrodes under the realistic PEMFC conditions.

4. Conclusions

In conclusion, we have shown that substantially improved ORR electrocatalysis occurs at a Pt_3Y alloy electrode and revealed the electronic effects of Pt_3Y alloys by using HR-XPS and XANES. We tested the Pt_3Y alloy catalysts under the realistic PEMFC conditions. Pt_3Y alloy nanocatalysts were fabricated by using an RF magnetron sputtering technique at high pressure with a mixture of gaseous Ar and He mixture gas. The Pt_3Y alloy nanocatalyst layer sputtered at 200 mTorr pressure consisted of nanoparticles with an average size of 10–12 nm. Multilayer sputtering with the application of the Nafion–carbon-ink on the surface after each sputtering was found to enhance the utilization of the catalysts. The fuel cell performance of Pt_3Y alloy nanocatalysts improved dramatically compared to that obtained with the Pt only nanoparticles. Our current research suggests possibilities for Pt_3Y alloy catalysts while simultaneously increasing the ORR activity in PEMFC.

Acknowledgments

This work was supported by E-Bank Project funded by KIST and by the Joint Research Project funded by KRCF, Korea. This work was also supported by the Global Frontier R&D Program on Center for Multiscale Energy System funded by the NRF under MEST (2011-0031571), Korea. YHC acknowledges a financial support by Priority Research Centers Program through NRF funded by MEST (2009-0093814), Korea.

REFERENCES

[1] Gasteiger HA, Kocha SS, Sompalli B, Wagner FT. Activity benchmarks and requirements for Pt, Pt-alloy, and non-Pt oxygen reduction catalysts for PEMFCs. Appl Catal B-Environ 2005;56:9–35.
[2] Dyer CK. Fuel cells for portable applications. J Power Sources 2002;106:31–4.
[3] Yoo SJ, Sung YE. Design of palladium-based alloy electrocatalysts for hydrogen oxidation reaction in fuel cell. In: Wieckowski A, Norskov JK, editors. Fuel cell science: theory, fundamentals, and biocatalysis. John Wiley & Sons Inc; 2010. p. 111–46.
[4] Savadogo O, Lee K, Oishi K, Mitsushima S, Kamiya N, Ota KI. New palladium alloys catalyst for the oxygen reduction reaction in an acid medium. Electrochem Commun 2004;6:105–9.
[5] Zhang J, Vukmirovic MB, Xu Y, Mavrikakis M, Adzic RR. Controlling the catalytic activity of platinum-monolayer electrocatalysts for oxygen reduction with different substrates. Angew Chem 2005;117:2170–3.
[6] Fernandez JL, Walsh DA, Bard AJ. Thermodynamic guidelines for the design of bimetallic catalysts for oxygen electroreduction and rapid screening by scanning electrochemical microscopy. M–Co (M: Pd, Ag, Au). J Am Chem Soc 2005;127:357–65.
[7] Koh S, Strasser P. Electrocatalysis on bimetallic surfaces: modifying catalytic reactivity for oxygen reduction by voltammetric surface dealloying. J Am Chem Soc 2007;129:12624–5.
[8] Toda T, Igarashi H, Uchida H, Watanabe M. Enhancement of the electroreduction of oxygen on Pt alloys with Fe, Ni, and Co. J Electrochem Soc 1999;146:3750–6.
[9] Greeley J, Stephens IEL, Bondarenko AS, Johansson TP, Hansen HA, Jaramillo TF, et al. Alloys of platinum and early transition metals as oxygen reduction electrocatalysts. Nat Chem 2009;1:552–6.
[10] Stamenkovic VR, Fowler B, Mun BS, Wang G, Ross PN, Lucas CA, et al. Improved oxygen reduction activity on $Pt_3Ni(111)$ via increased surface site availability. Science 2007;315:493–7.
[11] Nørskov JK, Rossmeisl J, Logadottir A, Lindqvist L, Kitchin JR, Bligaard T, et al. Origin of the overpotential for oxygen reduction at a fuel-cell cathode. J Phys Chem B 2004;108:17886–92.
[12] Zhang J, Vukmirovic MB, Sasaki K, Nilekar AU, Mavrikakis M, Adzic RR. Mixed-metal Pt monolayer electrocatalysts for enhanced oxygen reduction kinetics. J Am Chem Soc 2005;127:12480–1.
[13] Stamenkovic VR, Mun BS, Arenz M, Mayrhofer KJJ, Lucas CA, Wang G, et al. Trends in electrocatalysis on extended and nanoscale Pt-bimetallic alloy surfaces. Nat Mater 2007;6:241–7.
[14] Hirano S, Kim J, Srinivasan S. High performance proton exchange membrane fuel cells with sputter-deposited Pt layer electrodes. Electrochim Acta 1997;42:1587–93.
[15] O'Hayre R, Lee SJ, Cha SW, Prinz FB. A sharp peak in the performance of sputtered platinum fuel cells at ultra-low platinum loading. J Power Sources 2002;109:483–93.
[16] Cavalca CA, Arps JH, Murthy M.Fuel cell membrane electrode assemblies with improved power outputs and poison resistance. US Pat No 6300000 2001.
[17] Yoo SJ, Cho YH, Park HS, Lee JK, Sung YE. High utilization of Pt nanocatalysts fabricated using a high-pressure sputtering technique. J Power Sources 2008;178:547–53.
[18] Kitchin JR, Norskov JK, Barteau MA, Chen JG. Modification of the surface electronic and chemical properties of Pt(111) by subsurface 3d transition metals. J Chem Phys 2004;120:10240–6.
[19] Hammer B, Nørskov JK. Theoretical surface science and catalysis – calculations and concepts. Adv Catal 2000;45:71–129.
[20] Ganduglia-Pirovano MV, Natoli V, Cohen MH, Kudrnovsky J, Turek I. Potential, core-level, and d band shifts at transition-metal surfaces. Phys Rev B 1996;54:8892–8.
[21] Russell AE, Rose A. X-ray absorption spectroscopy of low temperature fuel cell catalysts. Chem Rev 2004;104:4613–36.